SHARAD MAPPING OF THE CALDERA OF ARSIA MONS. I. Ganesh[1], L. M. Carter[1] and I. B. Smith[2], [1]University of Arizona, Tucson, Arizona, USA (indujaa@lpl.arizona.edu), [2]York University, Toronto, Canada.

Introduction: Among the Tharsis Montes, only Arsia Mons shows signs of intra-caldera volcanism [1, 2]. The caldera floor hosts several small shields, vents, fissures and a network of lava flows dated to be 130 Ma old [3, 4]. Models of recurrence rates of volcanism based on the surface vents constrain the intra-caldera activity between 200–300 Ma and 90–10 Ma with vent creation rates peaking at 150 Ma [5]. The possibility of additional vents buried beneath the surface flows or a change in the style of volcanism from explosive to effusive eruptions ~150 Ma causes uncertainties in the increasing trend in vent production rate prior to 150 Myr [5]. Data from SHAllow RADar (SHARAD) can help in identifying and mapping buried volcanic deposits of distinct physical or petrochemical properties within the caldera. The dielectric structure of the subsurface as observed by SHARAD can be useful in elucidating the volcanic history of the caldera.

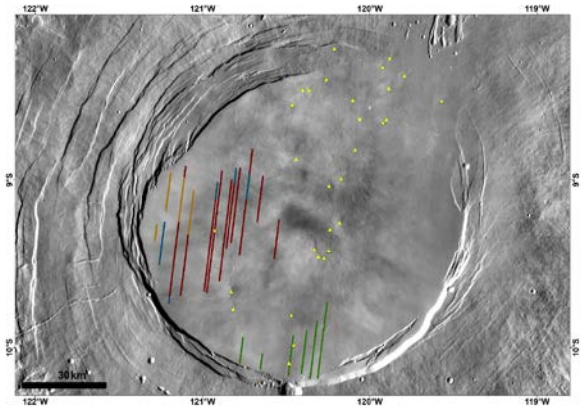

Figure 1: THEMIS day-IR image showing the locations of subsurface interfaces: Orange - dipping interfaces close to the surface; Maroon - flat interfaces underlying those shown in yellow; Blue - a second layer of flat interfaces directly beneath the first layer. Green - bright interfaces that occur close to the South caldera wall. Bright yellow triangles mark the locations of volcanic vents and fissures in the caldera.

SHARAD mapping: SHARAD is a sounding radar onboard the Mars Reconnaissance Orbiter (MRO) that operates at a 10 MHz bandwidth centered at 20 MHz [6]. This allows for range resolution of 15 m in free space and 5–10 m in geological medium [7]. SHARAD observations are processed into radargrams that display the return power as a function of signal return time along the y axis and along-track distance in the x direction. Radargrams from 27 night-time SHARAD tracks crossing the caldera were surveyed to locate late time delay echoes. Only those reflectors that were not apparent in the clutter simulations [8] were mapped as subsurface interfaces in order to avoid mapping clutter from off-nadir relief.

Mapping results: The reflectors (indicated by colored lines in Figure 1) do not lie close to the vent field (indicated by yellow triangles in Figure 1). The mapped interfaces are grouped into two based on their geographic location and subsurface structure. (1) The reflectors in the west show layering indicating radar backscattering from multiple vertically stacked dielectric interfaces. (2) The southern reflectors have high backscatter values almost equal to surface reflection, but do not show layering (Figure 2). The region between the surface echo and the subsurface echo in the radargram is dark and does not show any reflections.

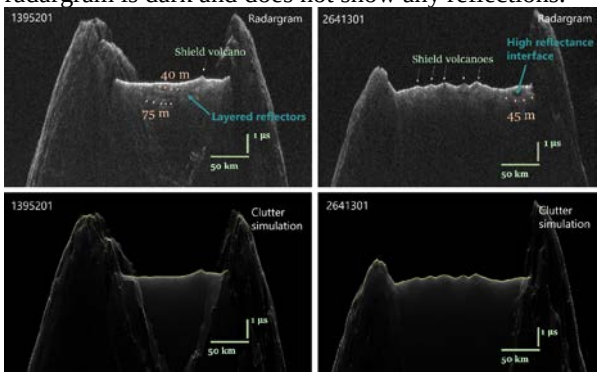

Figure 2: SHARAD radargrams (top) and clutter simulations (bottom) from track 13952 (left) and 26413 (right). The interface depths have been calculated assuming a dielectric constant (relative permittivity) value ε' = 7.

Bayesian inversion of SHARAD measurements: A Bayesian approach has been used to invert equations of time delay and return power to estimate the loss tangent *tanδ* and relative permittivity *ε'* of the subsurface media. Posterior probability distribution of *ε'* and *tanδ* were calculated using a maximum likelihood approach [9] without making any explicit assumptions about the media. The resulting distribution was then sampled by implementing a Markov chain Monte-Carlo (MCMC) technique using the Python package *emcee* [10] (resulting fit and posterior probability distribution are shown in Figure 3) to identify suites of solutions that are compatible with the signal return measured by SHARAD.

Dielectric properties of the subsurface:

Western interfaces. The layered interfaces in the west show increasing permittivity with depth. The topmost layers are 30-50 meters thick and the next set of interfaces lie 40-60 meters below the surface. The permittivity values are determined to be $\varepsilon' = 4.3 \pm 0.6$ for the upper layer, $\varepsilon' = 6.6 \pm 0.2$ for the second layer from the top and $\varepsilon' = 8.2 \pm 0.4$ for the lowest discerni-

ble layers (or half-space). The upper layer has a loss tangent value of $tan\delta = 0.019 \pm 0.003$ and the lower medium shows a higher loss tangent value of $tan\delta = 0.035 \pm 0.005$. The permittivity ε' of a medium can be linked to the medium's bulk density ρ through the relation $\varepsilon' = 1.96^{\rho}$ [11]. The increasing permittivity with depth therefore indicates an increase in bulk density of the subsurface layers. The permittivity estimations likely represents a subsurface structure with a thicker low-density medium overlying a relatively thinner high-density layer.

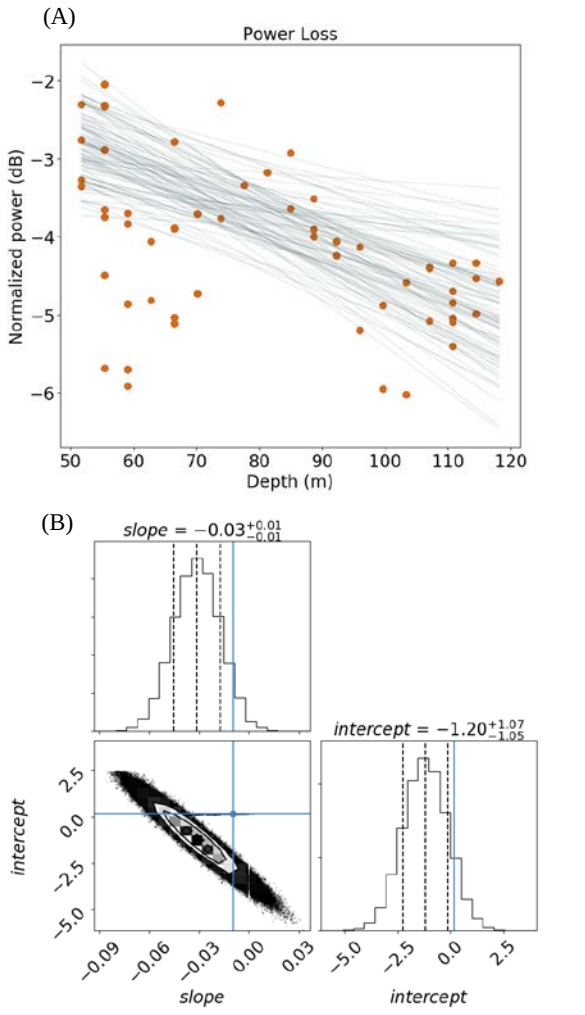

Figure 3: (A) Power loss as a function of depth for a 2nd layer reflector in track 22378. The brown circles are SHARAD data points; the gray lines are 100 randomly chosen samples from the MCMC model results plotted as linear fits to the data points. (B) Corner plot showing the 1-D and 2-D posterior probability distribution of the fit parameters (slope and intercept of the linear fit).

Southern interfaces. The bright reflectors in the south are 50-80 meters deep and have a very low permittivity layer with $\varepsilon' = 2.9 \pm 0.1$ above and a layer with permittivity of $\varepsilon' = 7.5 \pm 0.3$ below. The low permittivity for the upper layer combined with a thickness > 50 meters are consistent with deposits of volcanic ash, pumice or tuff [11]. The upper layers have loss tangent values of $tan\delta = 0.04 \pm 0.01$ indicating higher power loss compared to most of the western layers.

Implications for volcanism in the caldera: Mapping of the subsurface interfaces and Bayesian modeling of SHARAD signal propagation reveal differences in the properties of subsurface interfaces at different locations within the caldera. This could be due to differences in the style of volcanism through time in these two regions resulting in different types of buried deposits. The thickness of the surface dust layer could also influence the amount of signal transmitted through [12] and consequently alter the depth to which SHARAD can detect subsurface interfaces. The higher loss tangent in the south may also preclude the detection of any layers below the first interface.

The differences in the reflector properties (thickness, dielectric permittivity) most likely represent variations in eruption styles in the past. The lower layers in the western part of the caldera are possibly dense lava flows buried beneath a lower density medium that could be a vesicular lava flow or a mixture of effusive and explosive products. The unusually low permittivity values in the south are more indicative of ash or tephra overlying lava flows. The range of loss tangent values at both these locations are consistent with volcanic material. High values of dielectric loss for the lower layers in the west and the southern layers could be due to higher amounts of iron-bearing minerals in the subsurface [13]. Alternatively, volumetric scattering in the subsurface could also cause high loss tangent values. The differences in the subsurface structure provide confirmation that the style of volcanism was not uniform spatially and/or temporally within the caldera.

References: [1] Carr, M. H. et al. (1977) *JGR, 82*, 3985–4015. [2] Crumpler, L. S. and Aubele, J. C. (1978) *Icarus, 34*, 496-511. [3] Werner, S. (2009) *Icarus, 201*, 44–68. [4] Neukum, G. (2004), *Nature, 432*, 971–979. [5] Richardson, J. A. et al. (2017) *EPSL, 458*, 170–178. [6] Seu, R. et al. (2007) *JGR, 112*, E05S05. [7] Carter, L. M. et al. (2009) *GRL, 36*, L23204. [8] Choudhary, P. et al. (2016) *IEEE GRSL*, 13, 1285–1289. [9] Fisher, R. A. (1912), *Messenger Math., 41*, 155–160. [10] Foreman-Mackey, D. et al. (2012), *arXiv:1202.3665* [astro-ph.IM]. [11] Ulaby, F. T. et al. (1988), *Microwave dielectric spectrum of rocks*, Rep. 23817-1-T. [12] Simon, M. N. et. al. (2014) *JGR, 119*, 2291–2299. [13] Olhoeft G. R. (1998), *7th Intl. Conf. on GPR*, 177–182.

Acknowledgements: This work was partially funded by a SHARAD Co-I grant to L. M. Carter.